Toward Electron Encapsulation: Polynitrile Approach

Ilya A. Shkrob* and Myran C. Sauer, Jr.

Chemistry Division, Argonne National Laboratory, 9700 S. Cass Ave, Argonne, Illinois 60439

Received: January 30, 2006; In Final Form: April 27, 2006

This study seeks an answer to the following question: Is it possible to design a supramolecular cage that would "solvate" the excess electron in the same fashion in which several solvent molecules do that cooperatively in polar liquids? Two general strategies are outlined for this "electron encapsulation", viz. electron localization using polar groups arranged on the (i) inside of the cage or (ii) outside of the cage. The second approach is more convenient from the synthetic standpoint, but it is limited to polynitriles. We demonstrate, experimentally and theoretically, that this second approach faces a problem: the electron attaches to the nitrile groups, forming molecular anions with bent C−C−N fragments. Because the energy cost of this bending is high, for dinitrile anions in *n*-hexane, the binding energies for the electron are low and, for mononitriles, these binding energies are lower still, and the entropy of electron attachment is anomalously small. Density functional theory modeling of electron trapping by mononitriles in *n*-hexane suggests that the solute molecules substitute for the solvent molecules at the electron cavity, "solvating" the electron by their methyl groups. We argue that such species would be more correctly viewed as multimer radical anions in which the electron density is shared (mainly) between C 2p orbitals in the solute/solvent molecules, rather than cavity electrons. The way in which the excess electron density is shared by such molecules is similar to the way in which this sharing occurs in large di- and polynitrile anions, such as 1,2,4,5,7,8,10,11-octacyanocyclododecane^{-}. Only in this sense is the electron encapsulation possible. The work thus reveals limitations of the concept of "solvated electron" for organic liquids: it is impossible to draw a clear line between such species and a certain class of radical anions.

1. Introduction

In liquids that consist of molecules with no electron affinity, the excess electron sometimes exists as a metastable "solvated electron" in which the electron wave function occupies an interstitial cavity between several solvent molecules.[1,2] In polar liquids, such as water and alcohols, this cavity is lined by $-O^{\delta-}H^{\delta+}$ groups pointing toward the center of the cavity (Figure 1a).[3] Stabilization of the cavity electron through Coulomb attraction to permanent dipoles in the solvent molecules is opposed by repulsion due to the Pauli exclusion. To a first approximation, such a species can be regarded as a single quantum particle (the excess electron) in a classical potential well; this electron is treated separately from the valence electrons in the solvent molecules. The models of "solvated electron" differ chiefly in how this classical potential is implemented and various approximations made in the treatment of electron dynamics. The current state-of-the-art quantum mechanics−molecular dynamics (QM/MD) models of electron solvation [3] treat the liquid (usually, water) as an assembly of flexible, polarizable molecules (that are treated classically) and rigorously treat nonadiabatic dynamics of the electron in the fluctuating classical potential, which is prescribed (the electron is treated fully quantum mechanically).

Is the key simplification made in such one-electron models (the separability of a single quantum particle from the rest of the system that is treated classically) always sufficient to capture the observed properties of the "solvated electron"? The probable answer is no. A specific concern is that there might be a significant transfer of the excess electron density into the frontier orbitals of groups at the cavity wall. If such a transfer is not negligible, the core of the "solvated electron" should be more properly viewed as a multimer radical anion rather than a cavity electron. In our previous study,[4] we provided several arguments that such is indeed the case for the excess electron in liquid ammonia ("ammoniated electron") where the spreading of the negative charge onto N 2p orbitals of ammonia molecules in the first and second solvation shells is considerable, as suggested by density functional theory (DFT),[4] ab initio[5] calculations, and ^{14}N and ^{1}H NMR spectroscopy.[6] In practice, distinguishing between the cavity electron (in which most of the excess electron density is contained in a void between the solvent molecules) and a multimer radical anion (in which most of the excess electron density is in the frontier orbitals of several solvent molecules) may not always be possible, because there is no sharp boundary between these two modes of electron solvation.[7]

The dilemma of "cavity electron" vs "multimer radical anion" is especially vexing for organic liquids of no or low polarity, because permanent dipoles in the molecules are either lacking or weak, and the attractive potential originates entirely or mainly through the bond polarization. In water, the potential well for the "solvated electron" is >1.5 eV deep[2−4] and the electron wave function is largely contained within the potential well, with little electron density spilled over the outside (which justifies the use of the "solvated electron" picture for this liquid). In contrast, in liquid alkanes (such as *n*-hexane), the binding energy of the "solvated electron" is only 180−200 meV,[8,9] and the localization radius a of the exponentially decaying electron density $4\pi r^2\rho(r) \propto \exp(-2r/a)$ is ca. 4−5 Å.[9] This localization radius is larger than the radius of the cavity (3.2−3.6 Å), as determined from magnetic resonance data[10] for trapped electrons in vitreous alkanes and the reaction volume for electron localization in liquid and supercritical alkanes.[8] With the electron wave function

* To whom correspondence should be addressed. E-mail: shkrob@anl.gov.

10.1021/jp060638i CCC: $33.50 © 2006 American Chemical Society
Published on Web 06/08/2006

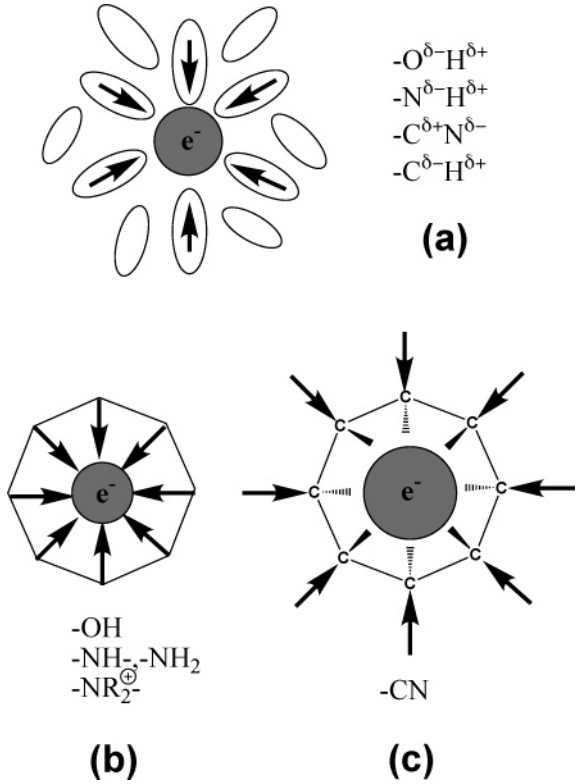

Figure 1. Conceptual drawing of (a) the solvated electron in a polar solvent, (b) encapsulated electron in the cavity of a cage with polar groups (such as −OH) arranged inside, and (c) the same as (b), with polar groups (−CN) arranged outside. The arrow symbolizes the positive end of the electric dipole pointing to the electron.

that diffuse, neglecting the interaction between the excess electron and valence electrons in the solvent molecules is poorly justified. Indeed, the existing models for solvated electrons in liquid alkanes have difficulty explaining the origin of the trapping potential.[11−13] The expected degree of polarization of alkane molecules appears to be insufficient to bind the excess electron. This persistent problem suggests that one-electron models may not suffice for the alkanes: the origin of the trapping potential might be the increased electron density in the frontier C 2p orbitals that weakens the C−C and C−H bonds and makes the alkane molecule more polarizable. The closer one examines such a "solvated electron", the more it resembles a radical anion.

The same question can be brought to a sharp focus by the following *Gedanke* experiment ("electron encapsulation"). Suppose that the entire first solvation shell of the solvated electron is replaced by a single supramolecular structure (the "cage") that has the internal cavity lined by polar groups (the conceptual drawing of such a cage is given in Figure 1b). The cage is suspended in a liquid with very low binding energy for the excess electron (such as an alkane or rare gas liquid). Assuming that the cage traps the excess electron, what is the result of this "electron encapsulation"? Should one regard the resulting species as a kind of "solvated electron" or as a large molecular anion?

The "electron encapsulation" is an experimental possibility. Electron trapping by hydrogen-bonded clusters of 2−4 alcohol molecules in nonpolar liquids has been studied by several groups,[14,15] We have recently demonstrated[15,16] that, due to the large dipole moment of acetonitrile (3.9−4 D vs 1.6 D for a typical alcohol), a single acetonitrile molecule can trap the electron in *n*-hexane and isooctane, apparently without the formation of a molecular anion. In both of these cases, one obtains a reducing species with absorption spectra and chemical properties that are indistinguishable from those of "solvated electrons" in neat liquids. Electron trapping by interstitial cavities that have well-defined, fixed geometry occurs in single crystals of carbohydrates (such as sucrose)[17] and in electrides.[18] In the former, trapped electrons with regular ligand geometry can be observed by using electron paramagnetic resonance (EPR) and optical spectroscopy. These observations suggest that "electron encapsulation" by a rigid supramolecular structure is possible.

The cage molecule should satisfy certain conditions that would preclude the formation of a molecular anion with the negative charge localized on the scaffolding. In particular, it should contain (1) no aromatic rings and C═C double bonds; (2) no C═O groups (with the possible exception of amide groups), halogen atoms (with the possible exception of F), and other electrophilic groups (such as nitro groups), and (3) no protons (e.g., quaternized amino groups) and other groups that rapidly react with the electron by, e.g., proton transfer. To deliver the electron to such a cage, one should be able to disperse these cages in solvents for which electron binding is very weak, such as (nonpolar) alkanes or (polar) hexamethyl phosphoramide.[19] The electron affinity of the cage should be larger than that of the solvent itself, as otherwise the electron would stay in the solvent.

The most difficult requirement to meet is that the polar groups should be arranged in such a way that the dipoles point toward the cavity center, with the positive charge closer to the center of the cavity (Figure 1b). In the vast majority of synthetic macrocycles (such as crown ethers, azacrowns, cryptands, etc.), the opposite is the case, because these macrocycles are *cation* rather than *anion* complexants. Thus, the search for a feasible cage for "electron encapsulation" naturally leads one to *anion* (especially, halide) receptors,[20,21] because the halide anions are solvated in a fashion that resembles electron solvation. Most of the anion receptors are polyammonium macro(bi)cycles that stabilize the interstitial halide (X^-) anion through Coulomb attraction to quaternized amino groups placed on ring, tetrahedral, or octahedral patterns (see Figures 1S, (a) to (d), in the Supporting Information).[20,21] In some of these macrobicycles (Figure 1S(b)), there is additional stabilization through the formation of $X^-\cdots H-N$ bonds.[22] Although recent experiments of Wishart and Neta[23] on solvated electrons in ionic liquids suggest that electron trapping by 3−4 fully functionalized $NR_4^{\oplus}$ cations might be possible, such "encapsulated electrons" would be the synthetic analogues of F-centers in ionic crystals rather than "solvated electrons" in organic liquids. Other, more exotic, classes of anion receptors (such as, for example, amide macrocycles,[24] Lewis acids (e.g., silacrowns),[20] and porphyrin-inspired[25] rings) do not fulfill the requirements stipulated above. Our exploratory studies indicate that without quaternization, azacrown, katapinand, and azacryptand macro(bi)cycles do not trap electrons in alkane solvents. The small negative enthalpy of such trapping, which can only occur via electron solvation by >N−H groups (that have small dipole moments <0.5 D), is insufficient to cancel a large loss in the entropy.

This examination suggests that the electron-trapping cavity can be lined only by highly polar groups, such as OH groups, to provide a sufficiently deep well for the electron. The design and synthesis of such a cage would be challenging, because the OH groups have to be arranged *inside* the cavity, whereas the natural preference for such groups is at the outside. Although there are structural motifs that can be explored (such as

cyclodextrins and their analogues), in this paper we focus on a different approach: using outward pointing >C−CN groups as electron-binding dipoles, as shown in Figure 1c. Because the positive charge in this dipole is on the carbon, such dipoles, when placed outside, still point toward the center of the cavity. The electron "solvation" is carried out by $>CH_2$ and/or >NH groups at the cavity walls. Because the dipole moment of the −CN group is large (3.9−4 D), such a placement still facilitates electron trapping by the cavity. Even in neat liquid acetonitrile[16,26] and $(CH_3CN)_n^-$ clusters,[27,28] the electron is solvated by *methyl* groups rather than cyano groups of the acetonitrile which point away from the cavity. A similar situation occurs for electrons in amides, where polar C═O groups also point away from the cavity.[19,29] (A review of electron localization in neat nitrile and dinitrile solids[30−33] and liquids[15,16,34] is given in Appendix 1 in the Supporting Information.) Thus, one can readily envision macro(bi)cycles with counter pointing cyano groups (such as the structures shown in Figure 2S(a),(b) in the Supporting Information). The electron occupies the cavity formed by methylene and amino groups; the stabilization of this cavity electron occurs via electrostatic binding to several CN dipoles placed outside of the cavity (Figure 1c).

The implementation of this scheme below, using transient photoconductivity method for evaluation of electron equilibria parameters (section 2), gave an unexpected result (section 3): placing just two cyano groups on the aliphatic scaffolding results in the formation of a molecular (monomer) anion instead of the anticipated "solvated electron" like species. Yet such molecular anions are not dissimilar to "solvated electrons" that occur in neat alkanes and mononitriles as suggested by our DFT calculations (section 4 and Appendix 3). As the number of nitrile groups arranged around the cavity increases, the anion begins to resemble the cavity type "solvated electron" more closely, but the complete transition to the cavity electron does not occur, either in the molecular or in the supramolecular structures.

2. Experimental Section

All chemicals were obtained in the purest form available from Aldrich and used without further purification; *n*-hexane (99+%) was passed through a 2 m long column filled with activated silica gel prior to use. The structures of (di)nitriles are given in Figure 3S in the Supporting Information. Other figures and sections with designator "S" can also be found therein. In the following, CH2N stands for *trans*-1,4-cyclohexanedinitrile (Figure 3S).

All measurements of electron dynamics were carried out using N_2-saturated solutions of *n*-hexane. The typical (impurity limited) lifetime of the electron was 300 ns. A representative set of the decay kinetics is given in Figure 2a (for glutaronitrile). The conductivity setup was the same as described in our previous publications.[9,15,16] The solution was placed in a 2 cm path optical cell with suprasil windows and ionized using two 248 nm photons from a KrF excimer laser (21 ns fwhm pulse, <0.1 J/cm^2). The second laser (Nd:YAG,1064 nm, 6 ns fwhm, <1 J/cm^2) was used to photoexcite trapped electron (or molecular anion), thereby injecting a quasifree electron into the conduction band of the liquid at a certain delay time t_L after the ionization event (50−500 ns; the time jitter between the two laser pulses was <3 ns). This photoexcitation yields a short-lived "spike" in the conductivity, as shown in Figure 2b, where the 248 nm induced signal has been subtracted from the signal obtained with both lasers. The decay of this spike represents reestablishment of the electron equilibria. The two laser beams propagated in the opposite directions and the 1064 nm beam completely enveloped the collimated 248 nm beam inside the conductivity cell. An electric field of 6−8 kV/cm was applied to two flat platinum electrodes spaced by 6.5 mm. The cell was placed in a metal jacket; the temperature of the photolyzed solution was controlled by circulating water containing antifreeze through this jacket. The photoconductivity signal $\kappa(t)$ was amplified and recorded on a transient digitizer with time resolution <2 ns. The conductivity is given in units of nS/cm ($10^{-7}\ \Omega^{-1}\ m^{-1}$); if not specified otherwise, the data were taken at 291 K (the "standard conditions" refer to 295 K). To determine the signal $\Delta\kappa(t)$ induced by the 1064 nm light, the Nd:YAG laser was pulsed on and off whereas the 248 nm laser was pulsed for every shot, and the difference signal was defined as $\Delta\kappa(t) = \kappa_{on}(t) - \kappa_{off}(t)$ (Figure 2b).

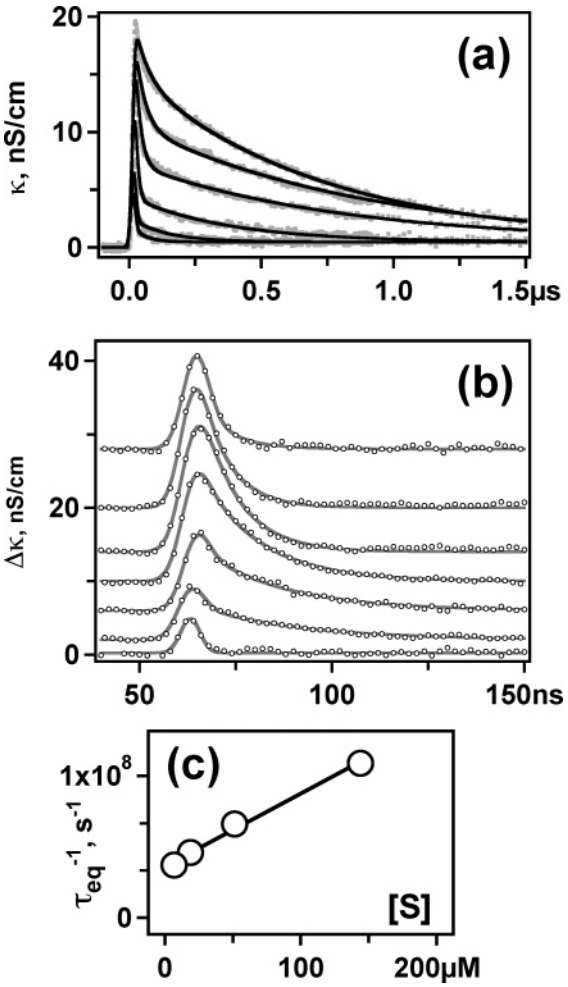

Figure 2. (a) Decay kinetics $\kappa(t)$ for two 248 nm photon induced transient conductivity signals from N_2-saturated *n*-hexane solutions (at 18 °C) containing (from top to bottom) 0, 6.7, 19, 52, 144, 380, and 1050 μmol/dm^3 glutaronitrile. The solid lines are multitrace least-squares fit obtained using eq (7S) in the Appendix 2. (b) Symbols: decay kinetics of 1064 nm induced "spike" in the photoconductivity ($\Delta\kappa$) obtained from the same solutions after laser excitation at $t_L \approx 62$ ns. The same concentrations as in (a), plotted from bottom to top. For convenience, the traces are stacked on top of each other. The solid lines drawn through the symbols are the least-squares fits obtained using eq 15S (Supporting Information). (c) Filled circles: concentration plot for the reciprocal time τ_{eq}^{-1} of settling equilibrium reaction 2 as determined from the analysis of kinetics shown in (b). [S] is the concentration of glutaronitrile, in μmol/dm^3. The slope of the line drawn through the symbols gives the rate constant of forward reaction 2.

3. Results

Typical decay kinetics for the photoconductivity signal observed after two 248 nm photon ionizations of *n*-hexane solutions (the (di)nitriles do not absorb at 248 nm) are shown in Figure 2a. The signal is from a mobile, quasifree electron e_{qf}^-, which is in thermodynamic equilibrium with the solvated electron

$$e_{solv}^- \rightleftarrows e_{qf}^- \quad (1)$$

This equilibrium is strongly shifted toward the left side: the lifetime of the localized (solvated) electron before it is thermally emitted back into the conduction band of the solvent is 8−10 ps,[9] whereas the trapping time of the quasifree electron is only 20−30 fs; i.e., it occurs even faster than the relaxation of its momentum (at 295 K).[9,35] The standard enthalpy of reaction 1 is ca. 0.2 eV.[8,9] Because the mobility of the quasifree electron is 10−100 $cm^2/(V\ s)$, whereas that of the solvated electron is only 10^{-4}−10^{-3} $cm^2/(V\ s)$, the conductivity signal is due to the small equilibrium fraction of the quasifree electrons. Due to the rapid settling of equilibrium reaction 1, this fraction tracks the concentration of solvated electrons, e_{solv}^-. The apparent lifetime of the conductivity signal is controlled by electron-accepting impurity, such as traces of oxygen and fluorocarbons. The conductivity signal decays exponentially as $\kappa(t) = \kappa_0 \exp(-k_0 t) + \kappa_i$, where κ_0 is rate constant for pseudo first order (irreversible) electron attachment to electron-scavenging impurity and κ_i is the conductivity signal from ions. The radical cation of *n*-hexane rapidly deprotonates;[36] the resulting cation has low mobility and makes negligible contribution to the overall conductivity signal. On the time scale of our kinetic observations (<2 μs), the loss of the electrons/ions due to their recombination in the bulk and migration in the electric field and discharge at the electrodes is negligible (the typical electron concentration was just a few nM).

In the presence of (di)nitriles, the electron reversibly reacts with the solute (*S*) yielding a product $\{e^-{:}S\}_{solv}$ (no specific structure is attributed to this product at this point):

$$e_{solv}^- + S \rightleftarrows \{e^-{:}S\}_{solv} \quad (2)$$

For 1,1-dinitriles (such as malono- and dimethylmalononitriles), the equilibrium is strongly shifted toward the product, so that backward reaction 2 is too slow to occur on the observation time scale. It is also possible that this attachment is dissociative, as occurs for electron attachment to the nitriles in *polar* solvents (the free energy gain due to the C−C bond dissociation is sufficiently great to exceed the large free energy loss due to the solvation of the small CN^- anion in the nonpolar medium).

Careful analysis of the decay kinetics suggests that for 1,2-, 1,3-, and 1,4- di-nitriles the product $\{e^-{:}S\}_{solv}$ reacts (with diffusion-controlled reaction rate) with another solute molecule yielding a C−C bridged dimer anion S_2^-:

$$\{e^-{:}S\}_{solv} + S \rightleftarrows S_2^- \quad (3)$$

The structure of this dimer anion should be similar to those of acetonitrile, succinonitrile, and adiponitrile dimer anions as observed by absorption spectroscopy and EPR[31−33] and suggested by quantum chemistry calculations.[26,33] reaction 3 shifts equilibrium (2) to the right side, which makes it necessary to take it into account to determine the equilibrium parameters of reaction 2. For glutaro- and succinonitrile (Figures 2 and 3, respectively), the rate constants for dimerization reaction 3 are close to those for diffusion-controlled reactions in *n*-hexane; for adiponitrile this reaction is ca. 10 times slower (Table 1). For mononitriles (see Figure 4 for butyronitrile), no evidence for the occurrence of reaction 3 has been found, as explained in refs 15 and 16. For these solutes, equilibrium is reached within the duration of the 248 nm laser pulse, so the amplitude of the exponentially extrapolated prompt conductivity signal κ_0 decreases as $(1 + K_{eq}[S])^{-1}$, where K_{eq} is the equilibrium constant of reaction 2;[15] the apparent rate of electron attachment to impurity also decreases, because the apparent mobility of the charge carrier decreases in the same proportion as the equilibrium fraction of solvated (and, therefore, quasifree) electrons.[9,15] Photoexcitation of $\{e^-{:}S\}_{solv}$ by infrared light causes electron detachment and injection into the conduction band of the solvent[15]

$$\{e^-{:}S\}_{solv} \xrightarrow{h\nu} S + e_{qf}^- \quad (4)$$

The released quasifree electron then undergoes reactions 1−3. Because the dimer anions have low cross-section for photodetachment at 1064 nm,[31,33] the initial magnitude of the signal $\Delta\kappa_0 = \Delta\kappa(t{=}t_L)$ induced by the 1064 nm light is proportional to the instantaneous concentration e_{solv}^- of solvated electrons in the reaction mixture immediately prior to the 1064 nm photon excitation at $t = t_L$. For mononitriles, the time profile of this prompt signal follows the $\kappa(t_L)-\kappa_i$ kinetics (of the electron decay) exactly. For dinitriles, the latter decay kinetics deviates at longer delay times (two examples of this behavior are shown in Figure 2b, for glutaronitrile, and Figure 4S, for CH2N), thereby indirectly supporting the occurrence of reaction 3. For mononitriles, settling of equilibrium (2) is very fast, and the conductivity signal $\Delta\kappa(t)$ induced by the 1064 nm light simply follows the time profile of the 1064 nm laser pulse. For dinitriles, the reactions are sufficiently slow that settling of the equilibrium following electron photodetachment (4) (or the initial photoionization) can be time resolved, and that allowed us to estimate

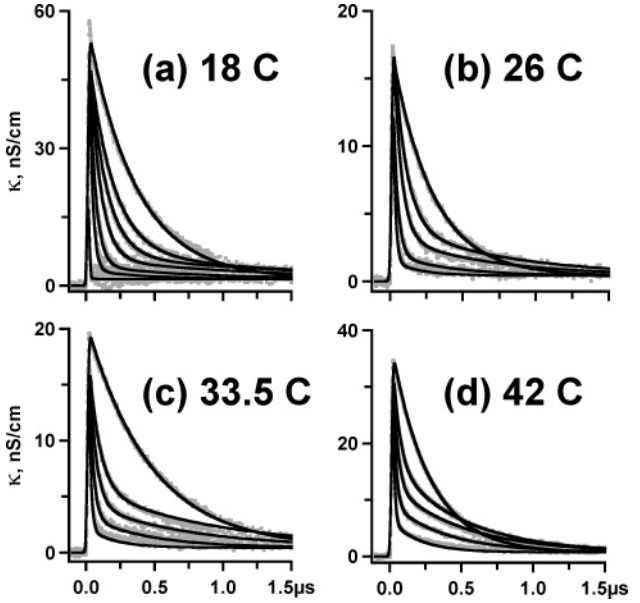

Figure 3. Decay kinetics of photoconductivity signal $\kappa(t)$ from an N_2-saturated solution of succinonitrile following two 248 nm photon ionizations of the solvent, at (a) 18 °C, (b) 26 °C, (c) 33.5 °C, and (d) 42 °C. The concentrations of the solute, in μmol/dm^3, were (from the top trace to the bottom trace in each series): (a) 0, 0.83, 1.67, 3.3, 6.7, 13.7, and 27.2, (b) 0, 2.8, 5.8, 12.4, and 27, (c) 0, 3, 5.9, 11.6, and 27, and (d) 0, 3.1, 6.2, 12.5, and 27. The solid lines are multitrace fits obtained using eq 7S in Appendix 2 of the Supporting Information.

TABLE 1: Experimental Thermodynamic and Kinetic Parameters for Reaction 2 in *n*-Hexane

solute	$-\Delta G°$, kJ/mol	$-\Delta S°$, J/(mol·K)	$-\Delta H°$, kJ/mol	$-\Delta H°$, meV	K_{eq},,[a] M^{-1}	$10^{11}k_2$,[a] M^{-1} s^{-1}	$10^{10}k_3$,[a] M^{-1} s^{-1}
acetonitrile	15 ± 2	15.4 ± 3	20 ± 1	200	470		
butyronitrile	12.5 ± 5	17 ± 8	17 ± 2	180	150		
adiponitrile	24 ± 4	61 ± 6	42 ± 2	435	16400	4.1	0.3
trans-1,4-cyclohexanedinitrile	23 ± 7	142 ± 12	66 ± 3	680	13000	6.8	
glutaronaitrile	26.6				46200	6.8	1.7
succinonitrile	35 ± 4	101 ± 7	66 ± 2	680	1.3×10^6	22	2.0

[a] At 295 K.

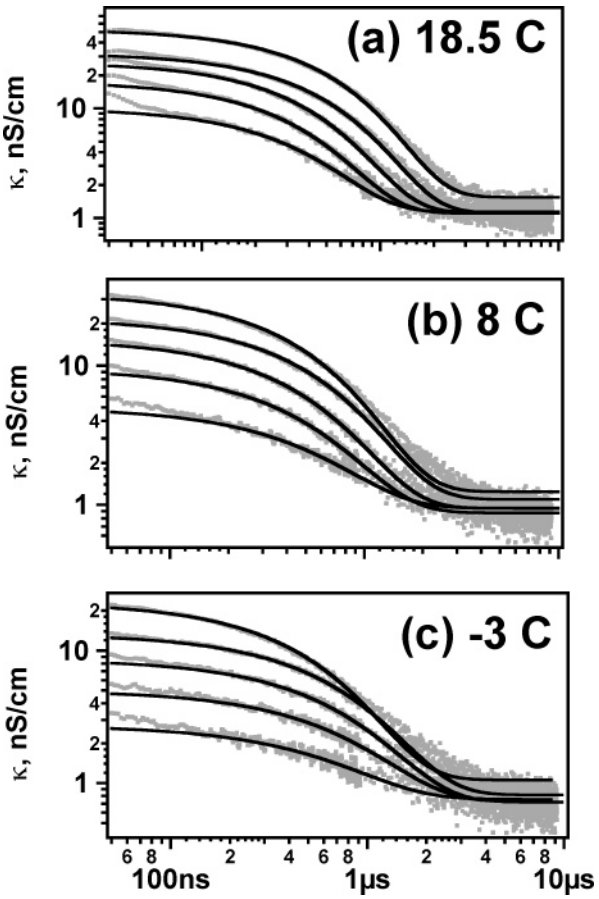

Figure 4. Same as for Figure 3, for butyronitrile at (a) 18.5 °C, (b) 8 °C, and (c) −3 °C. The concentrations of the solute were (from the top trace to the bottom trace in each series): 0, 3, 6, 12, and 23 mmol/dm^3. The solid lines are exponential fits; extrapolation of these fits to $t = 0$ gives κ_0. The equilibrium constant K_{eq} of reaction 2 can be obtained from the linear slope of the plot of $\kappa_0([S]=0)/\kappa_0$ vs [S], the molar concentration of butyronitrile.

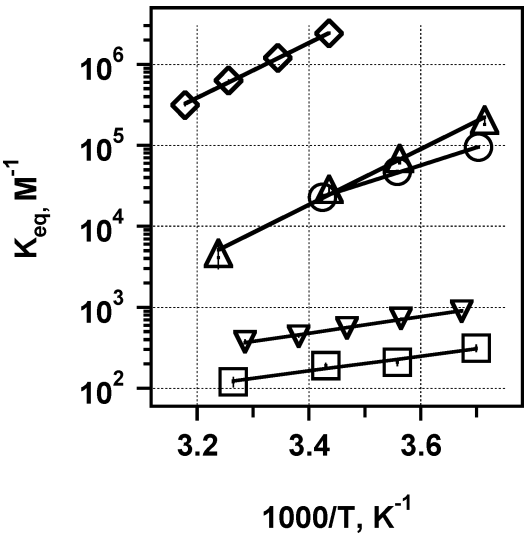

Figure 5. van't Hoff plot for molar equilibrium constants K_{eq} of reaction 2 vs reciprocal absolute temperature T, in K, for butyronitrile (□), acetonitrile (▽; data taken from ref 15, section 1S, Supporting Information), adiponitrile (○), CH2N (△), and succinonitrile (◇). The thermodynamic parameters for reaction 2 determined from these plots are given in Table 1.

the rate constants of forward and backward reactions 2 and reaction 3 directly. Relevant formulas are derived in the Appendix 2 given in the Supporting Information.

To derive the thermodynamics parameters of reaction 2, the families of decay kinetics for different concentrations [S] of the solute at several temperatures between −10 °C and +50 °C were analyzed (Figures 3, 4S, and 5S for succinonitrile, CH2N, and adiponitrile, respectively). The corresponding van't Hoff plots (Figure 5) of the equilibrium constant $K_{eq} = k_2/k_{-2}$ gave the standard enthalpy $\Delta H°$ and entropy $\Delta S°$ of reaction 2 at 295 K. For some solutes (especially, at elevated temperatures), the settling of the equilibrium was too rapid to resolve in time; in such instances the equilibrium fraction of e_{solv}^- was estimated from the extrapolated $\kappa(t)$ kinetics, and the equilibrium constant K_{eq} was determined from a linear correlation plot: $\kappa_0([S] = 0)/\kappa_0 = 1 + K_{eq}[S]$. In some instances, we were still able to estimate the settling time of reaction 2 from the "tails" the 1064 nm induced kinetics, as explained in ref 15 and the Appendix 2, because the 1064 nm pulse is much shorter than the 248 nm pulse (an example of such analysis for glutarontrile solution is shown in Figure 2b,c).

These kinetic and thermodynamic data can be summarized as follows: 1,1-dinitriles such as malononitrile and dimethylmalononitrile react with the electron rapidly and irreversibly (on our time scale) with rate constants of (0.63 ± 0.03) and $(1.04 \pm 0.05) \times 10^{12}$ M^{-1} s^{-1}, respectively (at room temperature). For comparison, reaction constants for electron scavenging by nitrobenzene, SF_6, CCl_4, CO_2, and N_2O (all of which are efficient electron scavengers) are 2.0, 2.0, 1.2, 1.8, and 1.5 $\times$ 10^{12} M^{-1} s^{-1}, respectively.[37] For succinonitrile, forward reaction 2 is also very rapid (Table 1); the rate constant is ca. 2.2×10^{12} M^{-1} s^{-1}. These rapid reactions suggest highly exoergonic electron attachment and indeed for succinonitrile the standard enthalpy of reaction 2 is large, ca. −0.68 eV, and the absolute free energy is the greatest among the dinitriles for which the thermodynamic data were obtained (Table 1). For other dinitriles, including malononitrile, forward reaction 2 is considerably slower, $(4-7) \times 10^{11}$ M^{-1} s^{-1}. Such relatively slow electron-attachment reactions were previously observed for solutes with low electron affinity, such as styrene (4.2×10^{11} M^{-1} s^{-1}), α-methylstyrene (6.3×10^{11} M^{-1} s^{-1}), and methylpentafluorobenzene (3.9×10^{11} M^{-1} s^{-1}), [37] all of which reversibly attach the electron and form molecular anions [38] (whose structure is well-known from matrix isolation EPR and absorption spectroscopy). The standard free energies of electron

attachment to styrene, α-methylstyrene, and difluorobenzene are −0.56, −0.51, and −0.33 eV, [38,39] respectively, which are significantly more negative than the free energies given in Table 1. The latter are close to the free energies of electron attachment to butadiene (−0.2 eV) as estimated by Holroyd[38] from high-pressure conductivity data. The standard enthalpies of electron attachment to styrene and α-methylstyrene (−1.1 eV)[39] are also much lower than those for the (di)nitriles in Table 1. Electron scavenging by the mono- and dinitriles thus appears to be the least exothermic reversible electron attachment reaction in *n*-hexane known to date. Actually, the standard heat of electron attachment to succinonitrile and CH2N (ca. −0.68 eV) is only slightly more negative than the standard heat of electron attachment to the ethanol tetramer cluster (ca. −0.57 eV);[15] for aceto-, butyro-, and adiponitriles, the electron attachment is less exothermic than that for the electron *solvated* by alcohol clusters in *n*-hexane! Such weakly exothermic electron attachment reactions have been observed previously only in *polar* media, where the energy of electron solvation is large. Consider, for instance, the attachment of solvated electron in tetrahydrofuran to benzene, for which the standard heat is −0.27 eV and the standard entropy is ca. −100 J/(mol·K).[40]

Using a pulse radiolysis−time-resolved conductivity method, Holroyd[39] obtained thermodynamic parameters for many electron attachment reactions that involve aromatic and olefin electron acceptors in alkane liquids. All such reactions have large negative standard entropy, between −85 and −200 J/(mol·K). For example, the standard entropies of electron attachment to styrene and α-methylstyrene in hexane are −186 and −207 J/(mol·K), respectively. For dinitriles, the standard entropy of reaction 2 is at the lower end of this range; for mononitriles the standard entropies are unprecedentedly low. To our knowledge, electron attachment reactions with such extremely low standard entropies have never been observed, in any liquid. This suggests that electron trapping by the mononitriles occurs in a different fashion from the dinitriles and other solutes that reversibly attach the electron in *n*-hexane: whereas the dinitriles form a molecular anion, the mononitriles undergo dipole binding to the solvated electron, as was first suggested in refs 15 and 16. The reason for such a divided pattern is examined below, using density functional theory models for the monomer and multimer radical anions.

4. Discussion

4.1. Computational Details. The basic computational approach used in this study is similar to that used in our previous publications, in particular, ref 4. Gas phase monomer and cluster anions were examined using DFT models with BLYP functional (Becke's exchange functional[41a] and the correlation functional of Lee, Yang, and Parr)[41b] from Gaussian 98.[42] This functional is most frequently used to estimate the energetics and hyperfine coupling constants (hfcc) in radicals and radical ions, for which it typically yields reliable results. We will use the hfcc's instead of the Mulliken spin and charge densities because the former can be experimentally determined using EPR and related spectroscopies. The isotropic part of the hfcc (A) is proportional to the s-character of the singly occupied molecular orbital (SOMO) for a given magnetic nucleus; the anisotropic part (only the largest principal value $2T$ of the anisotropic tensor is reported) is proportional to the magnetic dipole coupling of the unpaired electron to the spin of the magnetic nucleus.[43] In the point dipole approximation,[43] for a proton at a distance r from the electron at the center of a spherical cavity, $2T$ [G] $\approx 56.7/r^3$ [Å]. The hfcc's for ^{1}H, ^{13}C, and ^{14}N nuclei are given in units of G (1 G = 10^{-4} Tesla).

A 6-31G split-valence double-ζ Gaussian basis set augmented with diffuse and polarized functions was used for all calculations (6-31+G**). A ghost chlorine atom (i.e., a set of floating-center basis functions) at the center or a cluster was added. We also carried out second-order Møller−Plesset perturbation theory[41c] calculations using the same basis set and obtained comparable results to those obtained using the DFT methods (as was also the case with ammonia clusters). We emphasize that our star-shaped model cluster anions may not resemble at all the species observed in the gas phase.[4] The species of interest to us is the *core* of a much larger cluster anion which traps the electron in its interior, or the "solvated electron" in the bulk liquid. We focus only on those aspects of these DFT models of cluster anions that are likely to relate to the observed properties of the "solvated electron" in the liquid. For the same reason, we did not focus on the energetics of such gas phase clusters. Our scope is limited to only the *structural* properties of the core anion.

Because the definition of what constitutes the cavity in a many-electron model of "solvated electron" is ambiguous, the partition of the spin density between the cavity and the solvent molecules cannot be characterized in a unique fashion. Examination of isodensity maps for SOMO suggests that the electron wave functions inside the cavity and in C 2p orbitals of carbon atoms in methyl and methylene groups have opposite signs, which makes it easy to distinguish these two contributions. Qualitatively, this partition can be assessed by examination of isodensity contour maps of SOMO (like those shown below in sections 4.3 and 4.4, Figures 9−12). Typically, the diffuse, positive part of SOMO occupies 80−90% of the geometrical cavity at the density of +(0.01−0.12) a^{-3} and less than 10% at the density of +0.02 a^{-3} (where a is the atomic unit of length).

4.2. Molecular Anions of Mono- and Dinitriles. In gas phase mononitrile monoanions,[44,45] the electron is electrostatically bound to the CN dipole, with a diffuse wave function that has the spatial extent of several nanometers. Because we are not interested in such dipole-bound anions, a more useful model of the nitrile anion in a liquid is provided by a DFT calculation with a basis set that is deficient in very diffuse orbitals, such as the 6-31+G** set that was used in our calculations. The validity of such an approach is suggested by the ability of small-basis DFT calculations to capture all observable properties of monomer and dimer anions of acetonitrile in crystalline β- and α-acetonitrile, respectively.[33] The resulting optimized structures are shown in Figures 6−8; the structural parameters and energetics are summarized in Table 2, and calculated magnetic parameters (isotropic and anisotropic hfcc's) are given in Tables 1S and 2S in the Supporting Information. The adiabatic electron affinity (EA) given in the fourth column of Table 2 was defined as the difference in the energies between the lowest neutral and negatively charged nitrile molecules *in the same conformation.* For all dinitriles, the trans conformation in which the two CN dipoles are opposing each other is always the lowest energy one. The C−C−N angle strongly deviates from 180° for all (di)nitrile anions (Table 2), the C−N bond is elongated from 1.174 to 1.18−1.21 Å, and the C−CN bond is elongated from 1.47 to 1.49−1.52 Å. The degree of bending and bond elongation decreases with the size of the molecule, because these correlate with the degree of sharing of the negative charge with the alkyl/methylene groups. Figures 6−8 show the isodensity contour maps of the SOMO; it is seen from these maps and Table 1S that a large fraction of the spin density is contained in the N and C 2p orbitals of CN groups. The larger the bending angle, the more of the spin density is in these groups; for large

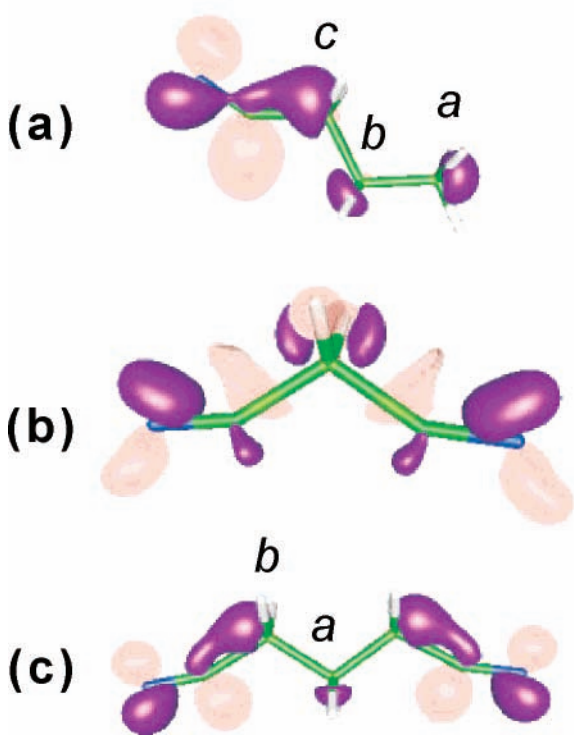

Figure 6. Isodensity contour maps of SOMO for radical anions of (a) butyronitrile, (b) malononitrile, and (c) glutaronitrile; for optimized geometry in the BLYP/6-31+G** model (gas phase). The lobes of different signs are purple and pink, respectively. The isodensity contours correspond to (a) ±0.04, (b) ±0.06, and (c) ±0.04 a^{-3}. The geometry and magnetic parameters are given in Table 1S in the Supporting Information.

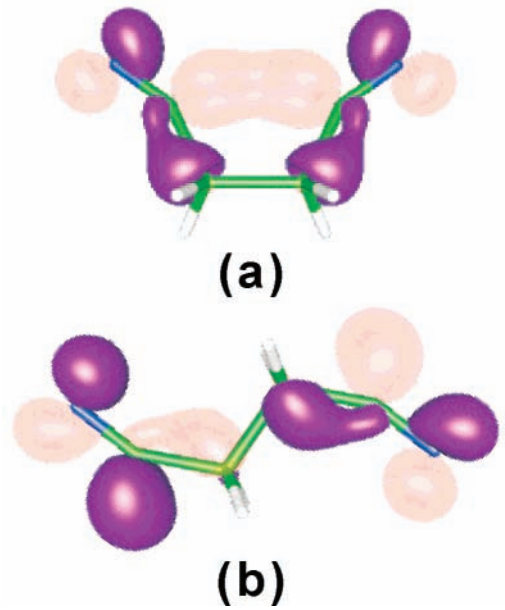

Figure 7. Same as for Figure 6, for (a) *syn* and (b) *anti* conformations of the radical anion of succinonitrile. Isodensity contours at ±0.05 a^{-3} are shown.

dinitriles (and polynitriles considered in section 4.5), the electron density spreads over, and the bending decreases.

For all of these (di)nitriles, the electron affinity as defined above is strongly negative (Table 2); the most negative is the EA for mononitriles (ca. −1 eV), the least negative are the EA for malono- and succinonitriles (−0.27 and −0.34 eV, respectively; Table 2). In a nonpolar liquid, such as *n*-hexane, the

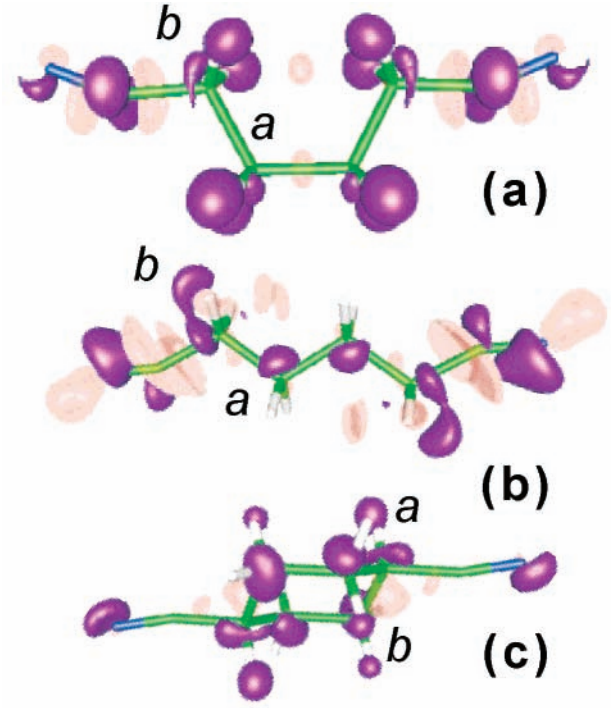

Figure 8. Same as for Figure 6, for (a) *syn* and (b) *anti* conformations of the radical anion of adiponitrile and (c) CH2N. Isodensity contours at ±0.04 a^{-3} are shown.

free energy for solvation of an anion is mainly determined by the Born polarization energy.[8] A better estimate of this solvation energy can be obtained using the polarized continuum method of Tomasi et al.; [46] this method was used in the integral equation formulation (IEFPCM). The solvation energy for the anions and corresponding neutral molecules (for their optimized gas phase geometries) are given in the fifth and sixth columns of Table 2, and the last column gives EA_{liq}, which is defined as the adiabatic affinity of a solvated nitrile molecule to the electron in a vacuum. Observe that all of these estimates are either very close to zero (for mononitriles) or positive (for dinitriles). Given that the V_0 (the energy of e_{qf}^- relative to the vacuum) for *n*-hexane is slightly positive (ca. 100 meV at 295 K)[8] and that e_{solv}^- is ca. 180−200 meV[8,9] lower in energy than e_{qf}^-, the adiabatic affinity of a solvated nitrile molecule to a quasifree/solvated electron is, respectively, 0.1 eV greater or 0.1 eV lower than EA_{liq}. It is seen from Table 2 that the largest absolute standard heat for reaction 2 is predicted for succinonitrile and malononitrile, in full agreement with the experiment. In particular, for malononitrile, the heat of electron attachment is so negative that the reaction would be irreversible on our time scale, as is indeed the case (section 3). The attachment is weakly exothermic for other dinitriles, but it is weakly endothermic for the mononitriles. Thus, the DFT calculations rationalize the pattern observed in section 3: for the dinitriles, the electron attachment with the formation of molecular anions with bent C−C−N fragments is sufficiently exothermic for reaction 2 to occur (Table 1). For the mononitriles, this type of electron stabilization is energetically prohibitive, and some other mechanism for electron localization sets in. We turn to the examination of this mechanism. The salient point of our examination is that the solvation modes in neat mononitriles and mixed mononitrile−alkane clusters are very similar to those in neat alkane clusters. Because the solvation in alkanes requires separate examination that is only peripherally connected with the main thrust of this study, this examination is placed in the

TABLE 2: Calculated Structural Parameters, Electron Affinity, and Free Energy of solvation of Mono- and Dinitriles and Their Anions[a]

solute	r(C−N), Å[b]	∠C−C−N, deg[b]	−EA, eV	$-\Delta G°$, eV (anion)	$-\Delta G°$, meV (neutral)	EA_{liq}, eV
acetonitrile	1.205	143.4 (*142.4*)[c]	1.00	1.07	62	≈0
butyronitrile	1.204	145.7	0.94	0.99	93	≈ −0.04
adiponitrile	1.192	154.5 (*157.2*)	0.52 (*0.44*)	0.88	173	0.188
trans-1,4-cyclohexanedinitrile	1.182	167.6	0.46	0.84	212	0.172
glutaronitrile	1.192	159.1	0.36	0.89	122	0.372
succinonitrile	1.205 (*1.195*)	151.7 (*152.2*)	0.34 (*0.19*)	0.98	90	0.514
malononitrile	1.192	152.5	0.27	0.95	153	0.59

[a] BLYP/6-31+G** calculation (refs 41 and 42); solvation energies are estimated using the IEFPCM method (ref 46); all conformations for dinitriles are lower-energy anti (trans) unless in italics. [b] In the same DFT model for neutral mono- and dinitriles, the length r(C−N) of the C−N bond is 1.174 Å and the C−C−N angle is 180°. [c] For the monomer anion of acetonitrile with methyl hydrogen and cyanide nitrogen in the syn position.

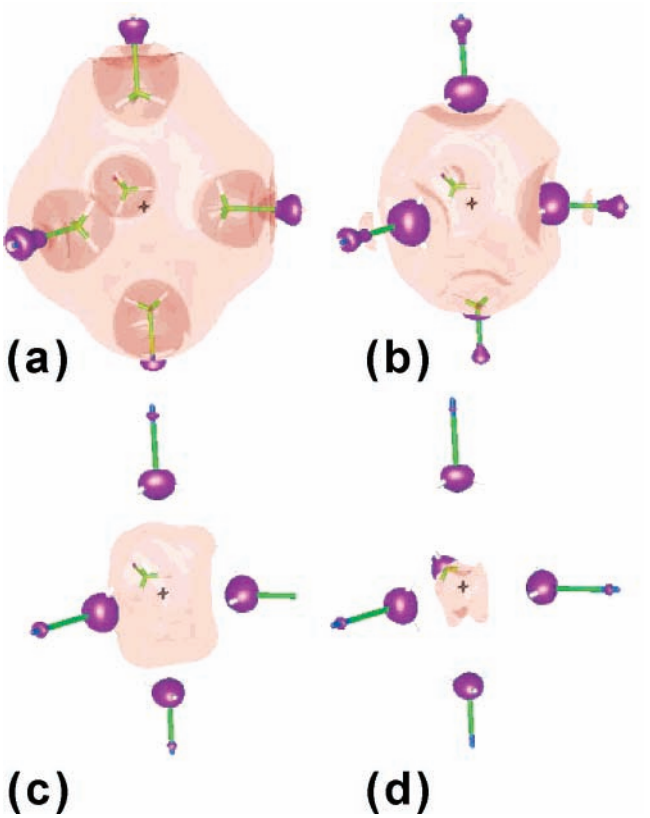

Figure 9. Isodensity contour maps of SOMO for the pentamer radical anion of acetonitrile for optimized geometry in the BLYP/6-31+G** model (gas phase). The lobes of different signs are purple and pink, respectively. The isodensity contours correspond to (a) ±0.008, (b) ±0.015, (c) ±0.02, and (d) ±0.026 a^{-3}.

Supporting Information (Appendix 3). We address the reader to this Appendix to the detailed discussion of the DFT model of the solvated electron in alkanes (implemented for ethane) and the comparison between this model and the experimental structural data.

4.3. Mononitriles. Liquid acetonitrile solvates the electron in a way similar to that observed in neat alkanes (exhibiting a broad absorption band in the near-infrared), and it is reasonable to expect that the electron is localized in a similar fashion. The DFT calculation for a star-shaped pentamer acetonitrile anion shown in Figure 9 validates this expectation. The spin density is divided mainly between the carbon atoms of methyl groups forming the cavity; some of this spin density fills the cavity.

TABLE 3: Geometry and Magnetic Parameters for Three Optimum Geometry Multimer Radical Anions (Figures 7S, 9, and 10)[a]

	$(C_2H_6)_5^-$	$(CH_3CN)(C_2H_6)_4^-$	$(CH_3CN)_5^-$
∠C−C−N = 180°		0.32	0.11 (0.27)
r(C−N)		1.175	1.174 (1.175)
r(C−CN)		1.472	1.471 (1.471)
r(C−H)	a 1.034 (1.1035) b 1.044 (1.1044)	ac 1.105 a 1.033 (1.034) b 1.041 (1.041)	1.103 (1.104)
r(X−H)	a 4.7 (3.42) b 7.05 (5.71)	ac 4.45[b] 4.45 (3.5)	4.22 (3.11)[c]
∠C−C−H	a 111.6 (111.7) b 111.4 (111.4)	111.6	110.8 (111.05)
$A(^{14}N)$		2.25	0.56 (0.66)
$A(^{13}C_N)$		0.86	1.17 (1.39)
$A(^{13}CH_3CN)$		55.4	26.7 (35)
$A(^{13}C_a)$	19.6 (19.11)	15.4 (17.9)	
$A(^{13}C_b)$	5.6 (3.89)	2.9 (1.42)	
$A(^1H_3C)$	a −0.69 (−0.7) b −0.33 (−0.405)	a −0.53 (−0.58) b −0.25 (−0.21)	−0.47 (−0.54)
$A(^1H_3C-CN)$		−1.0	−0.47 (−0.54)
$2T(^{14}N)$		0.11	0.07 (0.08)
$2T(^{13}CN)$		0.06	0.11
$2T(^{13}CH_3CN)$		0.15	0.14 (0.19)
$2T(^{13}C_a)$	0.51 (0.47)	0.38 (0.39)	
$2T(^{13}C_b)$	0.49 (0.41)	0.33 (0.31)	
$2T(^1H_3C)$	a 0.73 (0.81) b 0.39 (0.28)	a 0.57 (0.84) b 0.22 (0.18)	
$2T(^1H_3C-CN)$		1.33	0.68 (1.0)

[a] Bond distances and angles are given in Å and deg, respectively. Parameters for axial atoms are given first and for atoms in the plane second (in parentheses). For a neutral, C_{3v} symmetrical acetonitrile molecule r(H−C) = 1.1012 Å, r(C−C) = 1.4681 Å, r(C−N) = 1.1736 Å and ∠C−C−H = 110.3°. For a neutral, D_{3d} symmetrical ethane molecule, r(H−C) = 1.1029 Å, r(C−C) = 1.5435 Å, and ∠C−C−H = 111.37°. Symbols "a" and "b" relate to the innermost and outermost methyl groups in ethane molecules, symbol "ac" relates to the methyl group in acetonitrile molecule. [b] r(X−C) = 5.75 Å, r(X−N) = 7.08 Å. [c] r(X−C) = 4.79 Å, r(X−N) = 5.97 Å.

The average center of mass−hydrogen distance is 3.55 Å, but the SOMO is much more localized than the SOMO for the "solvated electron" in ethane (Figure 7S and Appendix 3). The changes in the molecular geometry as compared to neutral, isolated acetonitrile molecule are minor (the bond lengths are only 0.1−0.2% longer); see Table 3. The C−C−N angle is within 0.27° from 180°, as opposed to the monomer and dimer anions of acetonitrile (for which this angle is ca. 130°). This small bending explains the relative stability of the star-shaped solvation complex. The isotropic hfcc on methyl carbon-13 is 26.7 and 35 G (for axial and planar molecules); the hfcc's for other nuclei are significantly lower (Table 3).

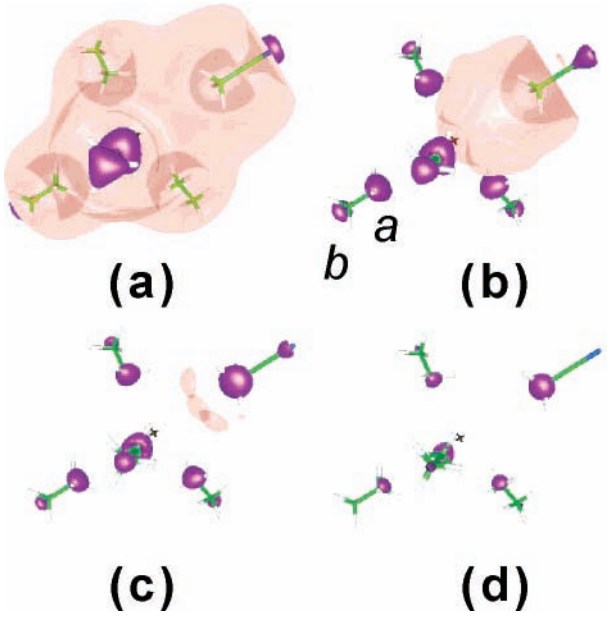

Figure 10. Same as for Figure 9, for a radical anion that includes four molecules of ethane and one of acetonitrile (placed radially on the long axis). The isodensity contours correspond to (a) ±0.01, (b) ±0.0175, (c) ±0.025, and (d) ±0.04 a^{-3}.

In Figure 10, a mixed cluster anion is shown in which acetonitrile substitutes for one of the ethane molecules (with ethane as a model alkane solvent; see Appendix 3). This substitution results in a surprisingly small change in the structure of the anion as compared to the ones shown in Figures 7S and 9. The C−C−N angle in the acetonitrile molecule is still very close to 180° (within 0.3°), and the changes in the geometry are minor (in a stark contrast to the acetonitrile monomer). The spin density is unevenly divided between the two carbons in the ethane molecules and the methyl carbon of acetonitrile. The isotropic hfcc constants on ^{13}C nuclei are 55.4 G (for $^{13}CH_3$-CN), 15−18 G (for C_a), and 1.5−3 G (for C_b), i.e., the spin density stays mainly at the cavity wall. The CN dipole is ca. 6.4 Å away from the cavity center (as compared to 6 Å estimated in ref 15 using the electron bubble model). The geometry and magnetic parameters for this cluster are given in Table 3. The conclusion is that with very minor geometry change, the acetonitrile molecule can participate in the network of alkane molecules that share the charge and form a multimer radical anion. The structure shown in Figure 10 is a radical anion, just like the structures shown in Figures 6−8, but the mechanism for the stabilization of this anion is different: the solute molecule shares the negative charge with the solvent molecules, undergoing almost no change in the geometry. In molecular anions shown in, e.g., Figure 8, the solute molecule accepts the whole charge on itself, which requires an extensive change in the geometry of the acceptor. For mononitriles, the first mode of electron localization prevails, hence the very small standard heat and entropy of reaction 2. For dinitriles, the molecular anion is formed instead, hence the large standard heat and entropy of reaction 2. However, the comparison of large dinitrile anions (CH2N) in Figure 8c and the composite cluster anion in Figure 10 suggest a remarkable degree of structural similarity. In the former anion, the C−C−N angle is only 12° smaller than 180°, and consequently, it shares many common features with the multimer anion shown in Figure 10. In both of these cases, the spin density is mainly in C 2p orbitals on the alkane chains. The specific way in which these spin densities are shared between the carbon atoms is different, because the aliphatic scaffolding is different, but the general pattern of the SOMO is the same. These two patterns become even more similar for the polynitrile anions examined next.

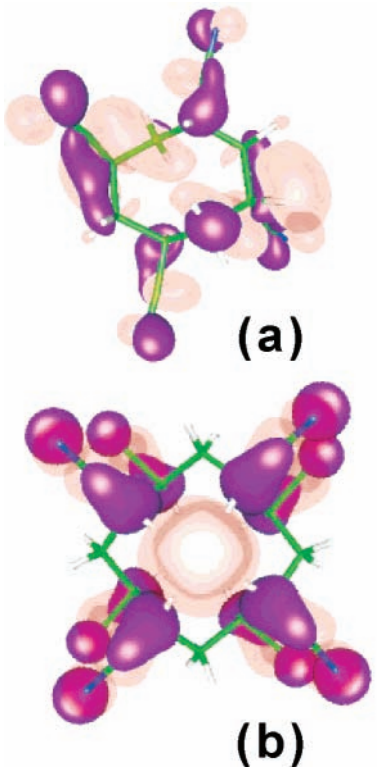

Figure 11. Same as for Figure 9 for radical anions of (a) 1,3,5,7-tetracyanocyclooctane and (b) 1,2,4,5,7,8,10,11-octacyanocyclododecane. The isodensity contours correspond to (a) ±0.025 and (b) ±0.02 a^{-3}. Both rings are nonplanar (the anions are shown from the top). See Figure 10S for a side view.

4.4. Polynitrile Rings. When several nitrile groups are placed on a cycloalkane ring, as shown in Figures 1c and 2S(a,b), the C−C−N angle becomes even closer to 180° (due to extensive negative charge sharing by the several nitrile groups) and the overall change in the geometry after the electron attachment becomes even smaller than that for the CH2N anion. Figure 11 shows isodensity SOMO maps for two polynitrile anions (whose structures were geometry optimized using the BLYP/6-31+G** method): 1,3,5,7-tetracyano-cyclooctane anion ($CO4N^-$) and 1,2,4,5,7,8,10,11-octacyano-cyclododecane anion ($CD8N^-$). More detailed maps are given in Figures 8S−10S in the Supporting Information, and the isotropic hfcc's are summarized in Figure 11S and Table 2S. The lowest energy $CO4N^-$ anion has C_i symmetry, and the $CD8N^-$ anion has D_4 symmetry. The estimated gas phase adiabatic electron affinity of the latter molecule is ca. 1.35 eV (B3LYP/6-31+G**) or 1.38 eV (B3LYP/6-311++G**). In the $CO4N^-$ anion, the C−C−N angles are 168.5° and 172°; for the $CD8N^-$ anion, all C−C−N angles are within 6° of 180°. Whereas relatively large C−C−N bending angles and small ring size preclude the formation of a "cavity electron" for $CH2N^-$ and $CO4N^-$ anions (Figures 11a and 8S), the SOMO maps for $CD8N^-$ reveal a dumbbell-shaped diffuse electron orbital filling the cavity (Figures 11b, 9S, and 10S). Although most of the spin density still resides in the C−C−N fragments (chiefly, on the carbons in the cyclododecane ring), as is the case with the smaller rings, the partitioning of the spin density between the cavity and the cyanide fragments is not too different from that observed for multimer radical anions shown in Figures 9 and 10. The orbitals on these C−C−N fragments resemble the orbitals for acetonitrile

molecules in Figures 9 and 10, though in $CD8N^-$ the SOMO exhibits more distinctive N 2p character (due to the bending of the C−C−N fragment). The electron cavity is formed by eight C−H groups whose protons alternate above and below the midplane of the ring (Figures 11b and 10S). The distance between the opposing >CH hydrogens is ca. 2.8 Å; i.e., the electron cavity is tight (for acetonitrile, the cavity radius was estimated to be ca. 3.55 Å). Consequently, the isotropic hfcc's on the protons are either slightly positive or slightly negative despite significant bond spin polarization involving C 2p orbitals (Table 2S). The isotropic hfcc's for cyanide ^{13}C and ^{14}N nuclei are small and positive, +0.43 G and +0.68 G, respectively (vs +1.5 G and +1.2 G, respectively, for the acetonitrile hexamer anion in Figure 9). The total hfcc for ^{13}C nuclei in the cyclododecane ring is ca. +110 G, whereas for methyl carbons in the hexamer anion shown in Figure 9 this parameter is ca. +160 G. Paradoxically, $CD8N^-$ more closely resembles the idealized "cavity electron" postulated by one-electron models than the solvated electron occurring in neat acetonitrile. Using computational models with more diffuse basis sets (such as B3LYP/6-311++G** and ab initio MP2/6-311++G** and HF/6-311++G** models) yields similar geometry and magnetic parameters for the optimized structures (Table 2S), suggesting that the picture of the electron localization on large polynitrile rings given above is robust.

In summary, in the multimer radical anion picture of the "solvated electron", $CH2N^-$ and the two polynitrile anions shown in Figure 11 might be viewed as the sought "encapsulated electron" because their general electronic structure is very similar to the structure of the (compound) multimer anions shown in Figures 9 and 10. For the $CD8N^-$ anion shown in Figure 11b, there is a "cavity electron" (Figures 9S(a,b) and 10S(a,b)) confined inside the ring. This "cavity electron" is stabilized by eight CN dipoles pointing toward the cavity center. Although the intracavity orbital carries only a fraction of the total spin density, such is also the case with the "solvated electron" occurring in neat alkane (Appendix 3) and acetonitrile solvents (section 4.3). Thus, a sharp division between these two classes of anions does not appear to exist: The "encapsulated electron" is a large molecular anion whose electronic structure strikingly resembles a radical anion commonly identified as the "solvated electron". Apart from this difference in terminology, there might be little difference in the nature of the species involved.

5. Conclusion

In this paper, we attempt to expand the concept of "solvated electron" to supramolecular structures. Two general approaches to electron encapsulation by a neutral molecule are recognized: a cage that is lined by polar groups on the inside of the cavity and a cage that has polar groups arranged outside of the cavity that dipole bind the electron. The latter approach makes it easier to design such a cage using organosynthetic methods, but it is feasible for polynitrile cages only. That prompted us to study electron attachment to mono- and dinitrile molecules dispersed in *n*-hexane, which has very low electron binding energy, thus allowing electron attachment to the solute. These studies indicated that electron trapping by mono- and dinitriles occurs in two different ways, as suggested by the thermodynamics of reaction 2: the dinitriles form a molecular (monomer) anion, whereas mononitriles substitute for a solvent molecule at the cavity of the "solvated electron". We then proceeded to model these two modes of electron attachment using DFT method. It was realized that the two ways of electron localization stem from the high energetic cost of bending the C−C−N fragment. This allows the formation of a molecular anion for dinitriles, where this bending is reduced due to the charge sharing between two nitrile groups but prohibits it for mononitriles, for which such a sharing cannot occur. As a result, the charge is shared instead with the *solvent* in a kind of extended radical anion analogous to the "solvated electron". This radical anion picture can also be applied to the "solvated electron" itself (in liquid alkanes), and it seems to produce a species whose SOMO exhibits all of the desirable features of the ground state wave function given by the electron bubble model that successfully rationalizes experimental observations (Appendix 3). This refinement of the standard "solvated electron" model makes new predictions as to the electron structure and magnetic parameters of the "solvated/trapped electron" in hydrocarbons.

The radical anion picture of the "solvated electron" in hydrocarbons developed in Appendix 3 readily rationalizes substitution at the cavity wall in the presence of mononitriles. Due to the extensive charge sharing between the molecules, very little change in the geometry of the solvent/solute molecules or the cavity size is needed to accommodate a nitrile molecule. The comparison of spin density maps for the mixed cluster anion shown in Figure 10 and large di- (e.g., Figure 8c) and polynitrile ring anions (Figure 11) suggests striking similarity between the ways in which the spin density is shared (mainly) by C 2p orbitals in both of these cases. If the central cavity in the polynitrile trap is sufficiently large and the C−C−N bending angle is reduced due to the extensive negative charge sharing between several nitrile groups, a feature resembling the "cavity electron" (as observed in Figures 9 and 10) emerges (Figure 11b). It appears that there is no conceptual difference between certain types of "solvated electrons" and "molecular anions", as these two are different realizations of the same motif for electron localization. In this sense, electron encapsulation by supramolecular structures is possible. On the other hand, the task of finding a supramolecular structure that experimentally implements (or closely approximates) the highly idealized "cavity electron" favored by one-electron models might be impossible. For polynitrile electron traps, this task is certainly impossible, as suggested by the results of the present study; for hydroxyl-lined cages (Figure 1b) discussed in section 1.1, the matter is still unsettled.

Apart from a purely academic interest, encapsulated electrons might present a technological one. Indeed, such a species would be the organic chemistry analogue of a semiconductor 3D quantum well or a quantum dot holding a single charge. Because trapped electron is largely decoupled from the magnetic nuclei in the solvent cage (such as the protons), the spin relaxation times are typically long, ranging from tens of milliseconds at 4 K to microseconds at 300 K. In contrast, decoherence times for electrons in semiconductor quantum dots are often shorter than 1 μs, even at 1−4 K. Furthermore, semiconductor dots/wells have multiple defects and exhibit a wide distribution of shapes and sizes that often preclude their reliable use in the circuitry; in contrast, electron trapping cages would be highly homogeneous in their properties, easy to manipulate in the solution, and easily modified and linked to other molecular structures.

Acknowledgment. I.A.S. thanks C. D. Jonah, R. A. Holroyd, J. F. Wishart, and F. T. Williams for many useful discussions and F.-P. Schmidchen, J.-M. Lehn, J. L. Dye, J. Sessler, and E. Anslyn for their advice and assistance. The initial impetus for this study was provided by a discussion with J. R. Miller that happened nearly 10 years ago. This work was supported by the

Office of Science, Division of Chemical Sciences, US-DOE under contract number W-31-109-ENG-38.

Supporting Information Available: A single PDF file containing Appendix 1: Electron trapping in nitriles; Appendix 2: Details of Kinetic Analysis; Appendix 3: "Solvated electron" in alkanes; Tables 1S and 2S; Figures 1S−11S with captions. This material is available free of charge via the Internet at http://pubs.acs.org.

References and Notes

(1) Shkrob, I. A.; Sauer, M. C., Jr. In *Charged Particle and Photon Interactions with Matter*; Mozumder, A., Hatano, Y., Eds.; Marcel Dekker: New York, 2004; p 301.

(2) Hart, E. J.; Anbar, M. *The Hydrated Electron*; Wiley-Interscience: New York, 1970. Coe, J. V. *Int. Rev. Phys. Chem.* **2001**, *20*, 33. Kevan, L. *Adv. Radiat. Chem.* **1974**, *4*, 181.

(3) Rossky, P. J.; Schnitker, J. *J. Phys. Chem.* **1988**, *92*, 4277. Schnitker, J.; Motakabbir, K.; Rossky, P. J.; Friesner, R. A. *Phys. Rev. Lett.* **1988**, *60*, 456. Webster, F. J.; Schnitker, J.; Frierichs, M. S.; Friesner, R. A.; Rossky, P. J. *Phys. Rev. Lett.* **1991**, *66*, 3172. Webster, F. J.; Rossky, P. J.; Friesner, R. A. *Comput. Phys. Comm.* **1991**, *63*, 494. Motakabbir, K.; Schnitker, J.; Rossky, P. J. *J. Chem. Phys.* **1992**, *97*, 2055. Rosenthal, S. J.; Schwartz, B. J.; Rossky, P. J. *Chem. Phys. Lett.* **1994**, *229*, 443. Murphrey, T. H.; Rossky, P. J. *J. Chem. Phys.* **1993**, *99*, 515. Schwartz, B. J.; Rossky, P. J. *J. Chem. Phys.* **1994**, *101*, 6917; *J. Phys. Chem.* **1994**, *98*, 4489. *Phys. Rev. Lett.* **1994**, *72*, 3282; *J. Chem. Phys.* **1994**, *101*, 6902. Wong, K. F.; Rossky, P. J. *J. Phys. Chem. A* **2001**, *105*, 2546. Borgis, D.; Staib, A. *Chem. Phys. Lett.* **1994**, *230*, 405. Staib, A.; Borgis, D. *J. Chem. Phys.* **1995**, *1995*, 2642. Borgis, D.; Staib, A. *J. Chim. Phys.* **1996**, *39*, 1628; *J. Chem. Phys.* **1996**, *104*, 4776; *J. Phys.: Condens. Matter* **1996**, *8*, 9389. Staib, A.; Borgis, D. *J. Chem. Phys.* **1996**, *104*, 9027. Borgis, D.; Bratos, S. *J. Mol. Struct.* **1997**, *1997*, 537. Nicolas, C.; Boutin, A.; Levy, B.; Borgis, D. *J. Chem. Phys.* **2003**, *118*, 9689. (b) Boero, M.; Parrinello, M.; Terakura, K.; Ikeshoji, T.; Liew, C. C. *Phys. Rev. Lett.* **2003**, *90*, 226403.

(4) Shkrob I. A. *J. Phys. Chem. A* **2006**, *110*, 3967.

(5) Newton, M. D. *J. Phys. Chem.* **1975**, *79*, 2795. Clark, T.; Illing, G. *J. Am. Chem. Soc.* **1987**, *109*, 1013.

(6) Catterall, R.; Stodulski, L. P.; Symons, M. C. R. In *Metal-Ammonia Solutions, Collogue Weyl II*; Lagowski, J. J., Sienko, M. J., Eds.; Butterworth: London, 1969; pp 151 and references therein. Niibe, M.; Nakamura, Y. *J. Phys. Chem.* **1984**, *88*, 5608. O'Reilly, D. E. *J. Chem. Phys.* **1964**, *41*, 3729. Holton, D. E.; Edwards, P. P.; McFarlane, W.; Wood, B. *J. Am. Chem. Soc.* **1983**, *105*, 2104. Catterall, R.; Stodulski, L. P.; Symons, M. C. R. *J. Chem. Soc. A* **1968**, 437.

(7) Symons, M. C. R. *Chem. Soc. Rev.* **1976**, *5*, 337.

(8) Holroyd, R. A. In *Charged Particle and Photon Interactions with Matter*; Mozumder, A., Hatano, Y., Eds.; Marcel Dekker: New York, 2004; p 175.

(9) Shkrob, I. A.; Sauer, M. C., Jr. *J. Chem. Phys.* **2005**, *122*, 134503.

(10) (a) Feng, D.-F.; Kevan, L.; Yoshida, Y. *J. Chem. Phys.* **1974**, *61*, 4440. (b) Narayana, P. A.; Kevan, L. *J. Chem. Phys.* **1976**, *65*, 3379.

(11) Hiraoka, K. *J. Phys. Chem.* **1981**, *85*, 4008. Kimura, T.; Fueki, K.; Narayana, P. A.; Kevan, L. *Can. J. Chem.* **1977**, *55*, 1940. Nishida, M. *J. Chem. Phys.* **1977**, *65*, 242.

(12) McGrane, S. D.; Lipsky, S. *J. Phys. Chem. A* **105**, *2001*, 2384. Funabashi, K. *Adv. Radiat. Chem.* **1974**, *4*, 103. Ichikawa, T.; Yoshida, Y. *J. Chem. Phys.* **1981**, *75*, 5432.

(13) Hammer, H.; Schoepe, W.; Weber, D. *J. Chem. Phys.* **1976**, *64*, 1253. Ichikawa, T. T.; Yoshida, H. *J. Chem. Phys.* **1981**, *75*, 5432.

(14) Mozumder, A. *J. Phys. Chem.* **1972**, *76*, 3824. Kenney-Wallace, G. A.; Jonah, C. D. *J. Phys. Chem.* **1982**, *86*, 2572. Baxendale, J. H. *Can. J. Chem.* **1977**, *55*, 1996. Baxendale, J. H.; Sharpe, P. H. G. *Chem. Phys. Lett.* **1976**, *41*, 440. Ahmad, M. S.; Atherton, S. J.; Baxendale, J. H. *Radiat. Radiat. Res., Proc. Int. Congr. 6th* **1979**, 220. Baxendale, J. H.; Rasburn, E. J. *J. Chem. Soc., Faraday Trans. 1* **1974**, *70*, 705. Baxendale, J. H.; Keene, J. P.; Rasburn, E. J. *J. Chem. Soc., Faraday Trans. 1* **1974**, *70*, 718. Gangwer, T. E.; Allen, A. O.; Holroyd, R. A. *J. Phys. Chem.* **1977**, *81*, 1469. Smirnov, S. N.; Anisimov, O. A.; Molin, Y. N. *Chem. Phys.* **1986**, *109*, 321.

(15) Shkrob, I. A.; Sauer, M. C., Jr. *J. Phys. Chem. A* **2005**, *109*, 5754.

(16) Shkrob, I. A.; Sauer, M. C., Jr. *J. Phys. Chem. A* **2002**, *106*, 9120.

(17) Lund, A. *Res. Chem. Intermed.* **1989**, *11*, 37 and references therein.

(18) Dye, J. L. *Annu. Rev. Phys. Chem.* **1987**, *38*, 271 and references therein.

(19) Rao, K. V. S.; Symons, M. C. R. *J. Chem. Soc., Faraday Trans. 2* **1972**, *68*, 2081. Brooks, J. M.; Dewald, R. R. *J. Phys. Chem.* **1968**, *72*, 2655. Mal'tsev, E. I.; Vannikov, A. V. *High Energy Chem.* **1971**, *5*, 337; *High Energy Chem.* **1974**, *7*, 338.

(20) Dietrich, B. *Pure Appl. Chem.* **1993**, *65*, 1457. Bianchi, A.; Bowman-James, K.; Garcia-Espana E. *Supramolecular Chemistry of Anions*; John Wiley−VCH: New York, 1997.

(21) Smith, P. H.; Barr, M. E.; Brainard, J. R.; Fird, D. K.; Freiser, H.; Muralidharan, S.; Reilly, S. D.; Ryan, R. R.; Silks, L. A., III; Yu, W. *J. Org. Chem.* **1993**, *58*, 7939; *Inorg. Chem.* **1995**, *34*, 569.

(22) Wishart, J. F.; Neta, P. *J. Phys. Chem. B* **2003**, *107*, 7261.

(23) Beer, P. D.; Gale, P. A. *Angew. Chem., Int. Ed.* **2001**, *40*, 486 and references therein.

(24) Schreerder, J.; Engbersen, J. F. J.; Reinhoudt, D. N. *Recl. Trav. Chim. Pays-Bas.* **1996**, *115*, 307.

(25) Xia, C.; Peon, J.; Kohler, B. *J. Chem. Phys.* **2002**, *117*, 8855.

(26) Mitsui, M.; Ando, N.; Kokubo, S.; Nakajima, A.; Kaya, K. *Phys. Rev. Lett.* **2003**, *91*, 153002.

(27) (a) Takayanagi, T. *Chem. Phys. Lett.* **2004**, *302*, 85. (b) *J. Chem. Phys.* **2005**, *122*, 244307.

(28) Shaede, E. A.; Dorfman, L. M.; Flynn, G. J.; Walker, D. C. *Can. J. Chem.* **1973**, *51*, 3905.

(29) Sprague, E. D. Ph.D. Thesis, University of Tennessee, June 1971, pp 115−117.

(30) Williams, F.; Sprague, E. D. *Acc. Chem. Res.* **1982**, *15*, 408. Bonin, M. A.; Chung, Y. J.; Sprague, E. D.; Takeda, K.; Wang, J. T.; Williams, F. *Nobel Symp.* **1972**, *22*, 103.

(31) (a) Bonin, M. A.; Takeda, K.; Tsuji, K.; Williams, F. *Chem. Phys. Lett.* **1968**, *2*, 363; *J. Chem. Phys.* **1969**, *50*, 5423. Campion, A.; Williams, *J. Chem. Phys.* **1971**, *54*, 4510. (b) Campion, A.; Ghormley, J. A.; Williams, F. *J. Am. Chem. Soc.* **1972**, *94*, 6301.

(32) Shkrob, I. A.; Takeda, K.; Williams, F. *J. Phys. Chem. A* **2002**, *106*, 9132.

(33) Bell, I. P.; Rodgers, M. A. J.; Burrows, H. D. *J. Chem. Soc.* **1976**, 315.

(34) Mozumder, A. *Res. Chem. Intermed.* **1999**, *25*, 243; *Chem. Phys. Lett.* **1993**, *207*, 245; *Chem. Phys. Lett.* **1995**, *233*, 167; *J. Phys. Chem.* **1996**, *100*, 5964.

(35) Stass, D. V.; Sviridenko, F. B.; Molin, Yu. N. *Radiat. Phys. Chem.* **2003**, *67*, 207.

(36) Table VII.4 & 5 in: Tabata, Y.; Ito, Y.; Tagawa, S. *CRC Handbook of Radiation Chemistry*; CRC Press: Boca Raton, FL, 1991; p 414.

(37) Holroyd, R. A.; Nishikawa, M. *Radiat. Phys. Chem.* **2002**, *64*, 19.

(38) Holroyd, R. A. *Ber. Bunsen-Ges. Phys. Chem.* **1977**, *81*, 298.

(39) Marasas, R. A.; Iyoda, T.; Miller, J. R. *J. Phys. Chem. A* **2003**, *107*, 2033.

(40) (a) Becke, A. D. *Phys. Rev. A* **1988**, *38*, 3098. (b) Lee, C.; Yang, W.; Parr, R. G. *Phys. Rev. B* **1988**, *37*, 785. (c) Møller, C.; Plesset, M. C. *Phys. Rev.* **1934**, *46*, 618. Frish, M. J.; Head-Gordon, M.; Pople, J. A. *Chem. Phys. Lett.* **1988**, *153*, 503; **1990**, *166*, 275; **1990**, *166*, 281.

(41) Frisch, M. J.; Trucks, G. W.; Schlegel, H. B.; Scuseria, G. E.; Robb, M. A.; Cheeseman, J. R.; Zakrzewski, V. G.; Montgomery, J. A., Jr.; Stratmann, R. E.; Burant, J. C.; Dapprich, S.; Millam, J. M.; Daniels, A. D.; Kudin, K. N.; Strain, M. C.; Farkas, O.; Tomasi, J.; Barone, V.; Cossi, M.; Cammi, R.; Mennucci, B.; Pomelli, C.; Adamo, C.; Clifford, S.; Ochterski, J.; Petersson, G. A.; Ayala, P. Y.; Cui, Q.; Morokuma, K.; Malick, D. K.; Rabuck, A. D.; Raghavachari, K.; Foresman, J. B.; Cioslowski, J.; Ortiz, J. V.; Stefanov, B. B.; Liu, G.; Liashenko, A.; Piskorz, P.; Komaromi, I.; Gomperts, R.; Martin, R. L.; Fox, D. J.; Keith, T.; Al-Laham, M. A.; Peng, C. Y.; Nanayakkara, A.; Gonzalez, C.; Challacombe, M.; Gill, P. M. W.; Johnson, B. G.; Chen, W.; Wong, M. W.; Andres, J. L.; Head-Gordon, M.; Replogle, E. S.; Pople, J. A. *Gaussian 98*, revision A.1; Gaussian, Inc.: Pittsburgh, PA, 1998.

(42) Dikanov, S. A.; Tsvetkov, Y. D. *Electron Spin−Echo Envelope Modulation (ESEEM) Spectroscopy*; CRC Press: Boca Raton, FL, 1992.

(43) Adrian, F. J.; Cochran, E. L.; Bowers, V. A.; Weatherley, B. C. *Phys. Rev.* **1969**, *177*, 129.

(44) For example: Abdoul-Carime, H.; Bouteiller, Y.; Desfrançois, C.; Philippe, L.; Schermann, J. P. *Acta Chem. Scand.* **1997**, *51*, 145. Desfrançois, C.; Abdoul-Carmie, H.; Adjouri, C.; Khelifa, N.; Schermann J. P. *Europhys. Lett.* **1994**, *26*, 25.

(45) Tomasi, J.; Persico, M. *Chem. Rev.* **1994**, *94*, 2027. Cancès, E.; Mennucci, B.; Tomasi, J. *J. Chem. Phys.* **1997**, *107*, 3032.